Nanostructure Characterization of Surface and Interface by FIB-SIMS and Photoelectron Diffraction

Yoshimasa Nihei

Institute of Industrial Science, University of Tokyo

(Received: Jan. 31, 1997 Accepted: Mar. 7, 1997)

Abstract

New frontier in material science have many problems in characterization and control of very small structures i.e. nanostructures especially in the fields of semiconductor devices and advanced optical, electrical and chemical materials. That is the main reason why the development of the methodology for characterization of nanostructure is so strongly needed. From the practical aspects every kinds of effort are carried out to apply the microbeam and surface sensitive method such as electron microscopy and surface spectroscopy. In this paper, our recent results on FIB-SIMS and Photoelectron Diffraction in X-ray region are introduced.

Secondary Ion Mass Spectrometry (SIMS) is well established as one of the most sensitive methods for local analysis. However, further improvements in spatial resolution and sensitivity are needed for the analysis of smaller volumes of materials. Recently, Ga Focused Ion Beam (Ga-FIB) have been developed and make possible to produce much higher current density beams with diameters < 0.03μm. Then, we can realize the higher spatial resolution SIMS by using Ga-FIB. In this paper, a simulation method for erosion of a solid by FIB bombardment and microparticle analysis using the Ga-FIB SIMS is described.

Photoelectron diffraction in X-ray region is a recently developed method and one of the most powerful tools for the structural analysis of solid and interfaces in atomic scale. The angular distribution curves of photoelectron spectra bring us very fruitful information on the structure of materials because photoelectron spectra can resolve the energy states of the element, chemical bond and electron spin. In this paper, our results on the high resolution photoelectron diffraction and on the structural analysis of initial stage of epitaxial layer growth are described.

1. Introduction

New frontier in material science have many problems in characterization and control of very small structures i.e. nanostructures especially in the fields of semiconductor devices and advanced optical, electrical and chemical materials such as quantum effect devices, chemical sensors and catalysts. That is the main reason why the development of the methodology for characterization of nanostructure is so strongly needed. On the other hand, in order to analyze the nanostructure, we need to realize atomic to submicron resolution in lateral and in depth direction. From the practical aspects every kinds of effort are carried out to apply the microbeam and surface sensitive methods such as electron microscopy and surface spectroscopy. In this paper, our recent results on FIB-SIMS and Photoelectron Diffraction in X-ray region are introduced.

Secondary Ion Mass Spectrometry (SIMS) is well established as one of the most sensitive methods for local analysis. Using of O^+, O_2^+, O^-, Cs^- ions as a primary beam, many studies for material characterization have been carried out. Quantification in SIMS analysis have also bean widely investigated and greatly advanced[1-4]. However, further improvements in spatial resolution and sensitivity are needed for the analysis of smaller volume of materials. Recently, Ga Focused Ion Beam (Ga-FIB) have been developed and make possible to produce much higher current density beams with diameters < 0.03μm. Then, we can realize the higher spatial resolution SIMS by using Ga-FIB. Moreover, Ga-FIB can be used for machining tool because of its high current density. Then, we can carry out three dimensional elemental analysis by combining of nano-scale machining tool and high resolution elemental mapping techniques. In this paper, a simulation method for erosion of a solid by FIB bombardment and microparticle analysis using the Ga-FIB SIMS are described.

Photoelectron diffraction in X-ray region is a recently developed method and one of the most powerful tools for the structural analysis of solid and interfaces in atomic scale. The angular distribution curves of photoelectron spectra bring us very fruitful information on the structure of materials because photoelectron spectra can resolve the energy states of the element, chemical bond and electron spin. This really unique method can detect simultaneously the energetic character and structural character.

In this paper, results on the high resolution photoelectron diffraction and on the structural analysis of initial stage of epitaxial layer growth are described.

2. Apparatus

2.1 Ga-FIB SIMS

In order to improve the spatial resolution of SIMS, the narrower and brighter ion beam such as FIB is needed. Because of the higher sputtering rate of FIB, however, the signal intensity of SIMS changes very rapidly. Therefore, in order to get quantitative and integrated intensity of secondary ions, and the ratio of them, the simultaneous detection of multiple elements would be required. This kind of detection system will bring us the another advantage such as higher efficient detection of secondary ions. As shown in Fig. 1, the apparatus consists of a primary ion optical column, a secondary electron detector, secondary ion transfer optics including a total secondary ion detector, a plane-focusing mass analyzer equipped with multichannel ion detection system, and control electronics [5]. Field-emitted Ga^+ ions are accelerated to 35 keV and focused on the sample. The beam diameter on the sample is estimated to be < 0.1μm for a 100pA beam current; the primary beam density is estimated to be ~ $1 A/cm^2$. Therefore, both high-spatial resolution and large sputtering rate are realized.

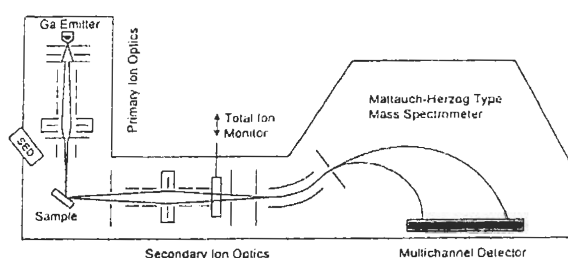

Fig. 1 Ga-FIB SIMS apparatus equipped with multichannel ion detection system.

2.2 High-angular-resolution X-ray Photoelectron Diffraction (XPED)

Measurements were performed using an angle-resolved X-ray photoelectron spectrometer equipped with a multichannel hemispherical electron energy analyzer and a high-precision manipulator for specimen rotation. The detection angle of the analyzer was restricted by an array of microchannels in front of the electrostatic entrance lens. The mean deviation of the detection angle can be selected from 0.3 to 1.3 degree [6].

3. Results and Discussion

3.1 Erosion of a Particle by FIB Bombardment

Sputtering yield of a solid largely depends on the incident angle of ion beam. This is a serious problem in the analysis of particulate samples. In the case of a rastered FIB bombardment, the uneven erosion of a particle occurs because of the change in the incident angle at each part of a particle. In the shave-off scan[7], it was experimentally found that the topographic effect is negligible. Therefore, by using the shave-off scan, the cross-sectioning of a particulate sample can be performed. In order to clarify the property of the cross-sectioning, a three-dimensional simulation method of the erosion of a solid was established. In this paper, the shape of the cross-section of a spherical particle in the shave-off scan mode is discussed using the simulation.

3.1.1 Simulation Procedure

Major factors concerning the shape of an eroded surface are the incident angle dependence of sputtering yield $S(\theta)$ and the redeposition of sputtered materials onto the surface. Our main interest is the shape of the cross-section. Because the redeposition affects the shape of side walls facing the sputtering plane, only the effect of $S(\theta)$ function on the eroded shape was taken into account in the simulation. The simulation procedure is as follows. i) A sample including its internal structure is expressed by a set of 3-D spaced point elements. Each sample point element contains two parameters; the number of atoms contained in a point element N (x, y, z) and the sputtering yield at normal incidence S (0). ii) Arbitrary scanning pattern of an FIB and the current distribution within the beam spot are expressed by giving the fractional beam current I (x, y) to each of the beam point elements. iii) Sputtering is performed by reducing N (x, y, z) in each sample point as $\Delta t I$ (x, y) $S(\theta)$, where Dt is the beam passing period for a sample point element. As for the expression of $S(\theta)/S(0)$, an analytical formula was assumed.[8] When N (x, y, z) is less than zero, the sample point element is completely sputtered out. Process iii) is repeated for the total bombardment time.

3.1.2 Erosion of a Particle by Shave-off Scan

Using the simulation, the property of the erosion of a spherical particle just half buried on a plate was examined. Figure 2 shows the eroded shapes during the FIB bombardment in the shave-off scan mode. The ratio of the scanning frequencies for *X* and *Y* direction was 10^4 : 1. Each of the cross-section was close to a flat plane except a little bend towards *Y* scanning direction. Because the residual shape of the eroded part kept its initial (spehrical) shape, it could be considered that there was little topographic effect. Cross-sectional profiles along *Y* direction were shown in Fig. 3. The profile of the cross-section did not change during the cross-sectioning. This means that the shave-off scan can perform the precise cross-sectioning independent of the initial shape of the sample. Furthermore, the intermittent cross-sectioning gives flat planes for lateral analysis at arbitrary position of a particle. Therefore, the combination of the cross-sectioning and the lateral analysis of the cross-sections realizes a fully 3-D analysis of particulate samples.

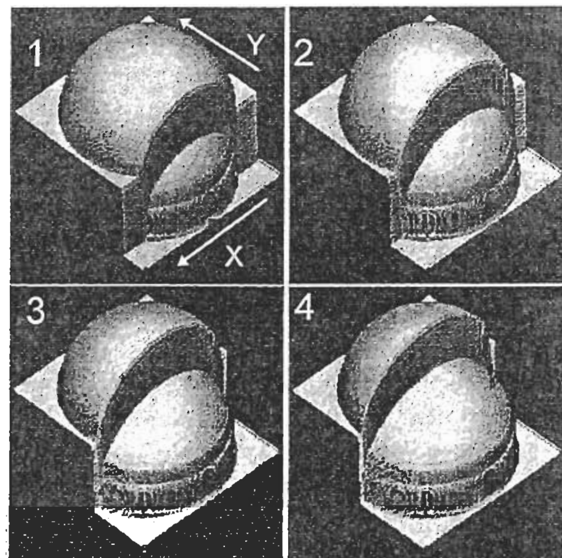

Fig. 2 Cross-sectioning of a particle half buried on a plate. (After shave-off scan for 1) 270s, 2) 404s, 3) 538s, 4) 673s, FIB: 0.2μmφ, 200pA)

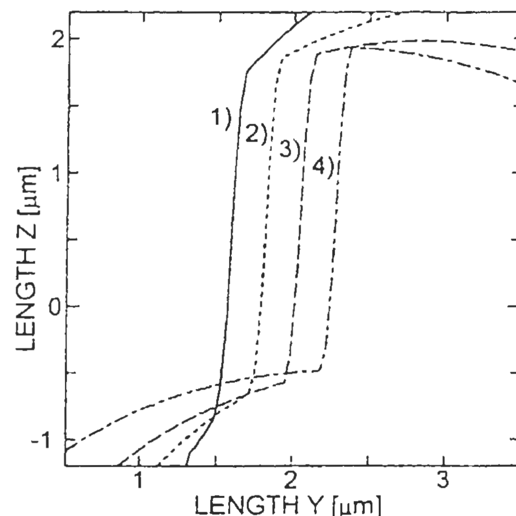

Fig. 3 Profiles towards *Y* scan direction at each period shown in Fig.1. Profiles were relatively plotted to compare with one another.

3.2 Analysis of Nonmetallic Inclusion in Steel

Nonmetallic inclusions frequently exert unfavorable influences on the quality of steel. It is desirable to clarify the origin and generation process of inclusion particles. In order to measure the shape, size, composition and inner elemental distribution, it is necessary to develop characterization methods for each inclusion particle. The author presents a novel characterization method using Ga-FIB SIMS. The sample is Al-deoxidized and Ti-denitrified low carbon steel. The inclusion particles were segregated onto the surface of the steel by electron beam melting. The inclusion particles were analyzed individually by using electron probe microanalysis (EPMA) and Ga-FIB SIMS. At the first, a hundred particles were analyzed by EPMA, and the average composition of each particle was obtained. Based on these data, we performed multivariant cluster analysis for 100 particles. After that, we carried out a shave-off analysis for single particle by Ga-FIB SIMS. The primary ion beam diameter and current were 0.2μm and 120pA.

From EPMA measurements, the inclusion particles were classified into 3 types. The number of particles in each cluster was as follows: 83 particles in cluster 1, 12 particles in cluster 2 and 5 particles in cluster 3. The shave-off analysis was applied to typical particles in each cluster. Figure 4 shows the SEM images, X-ray spectra and shave-off profiles of a single inclusion particle in each cluster. From the shave-off analysis, the composition and inner elemental distribution were obtained. The inner elemental distribution seems to be homogeneous in the particle classified into cluster 1 and 3. On the other hand, it is obvious that the profiles of $^{48}Ti^+$, $^{41}AlN^+$ and $^{43}AlO^+$ in cluster 2 are different from the other profiles. Thus, the inner distribution was inhomogeneous in the particle in cluster 2.

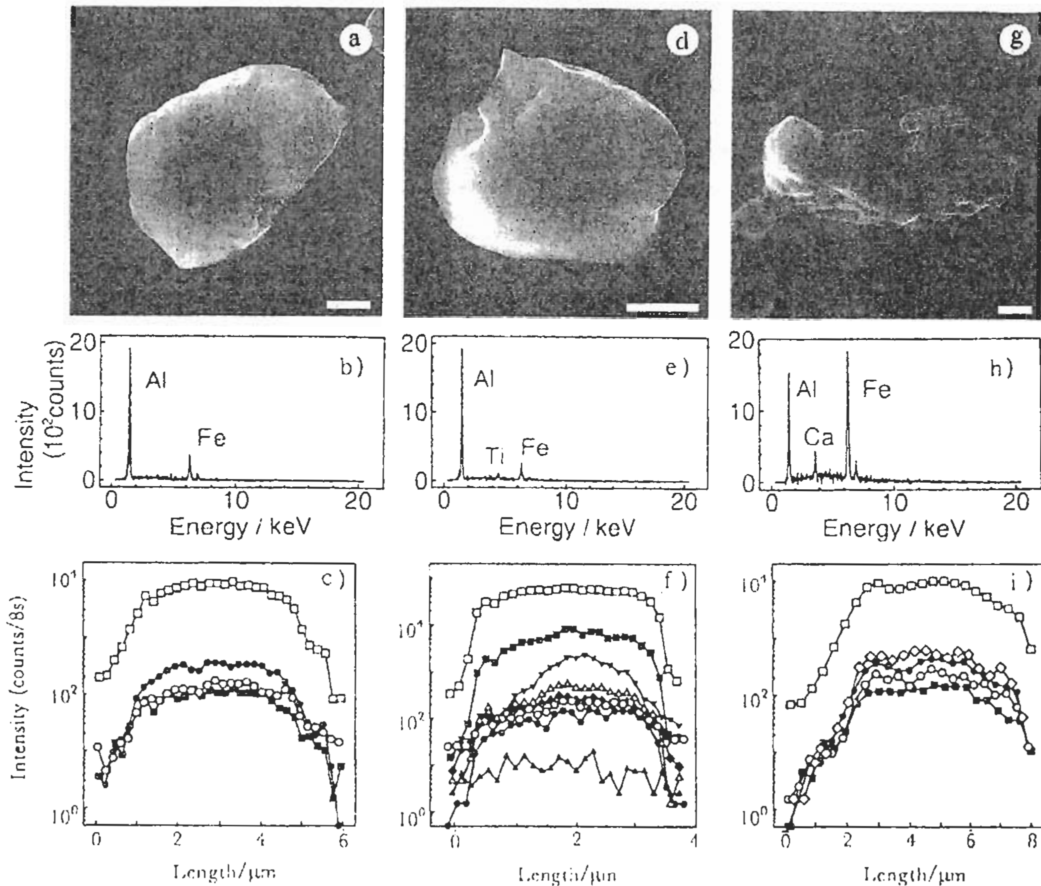

Fig. 4 SEM images, X-ray spectra and shave-off profiles of typical inclusion particle. (a,b,c): cluster 1; (d,e,f): cluster 2; (g,h,i): cluster 3; scale bar: 1μm; ●: intensity of $^{14}N^+$; ○: $^{16}O^+$, ■: $^{23}Na^+$; □: $^{27}Al^+$; ◆: $^{28}Si^+$; ◇: $^{40}Ca^+$; ▲: $^{41}AlN^+$; △: $^{43}AlN^+$; ▼: $^{48}Ti^+$.

Sodium atoms in nonmetallic inclusion particles are known to be in the phase of $xNa_2O.ySiO_2$. In the shave-off analysis, the number of Si atoms was proportional to the number of Na atoms. From the ratio of Si atoms to Na atoms, it was concluded that Na and Si in the particle were shown to form the phase of $Na_2O.2SiO_2$. Intensities of $^{23}Na^+$ and $^{28}Si^+$ were used to calculate the $Na_2O.2SiO_2$ fraction, $^{43}AlO^+$ to Al_2O_3 fraction, and $^{41}AlN^+$ to AlN fraction. Because Ti was added after deoxidization by Al, only TiN was the expected chemical form Ti could have. Therefore, the fraction of TiN was calculated from the $^{48}Ti^+$ intensity. The results of composition analysis are listed on table at several different cross-sections in each particle classified into cluster 2. The corresponding position is shown in Fig. 5. The major compound was Al_2O_3 at any of three cross-sections. Aluminum nitride had a higher concentration at cross-section A, B and D. Titanium nitride had a higher concentration at cross-section C, E and F.

From these analyses, the generation process of nonmetallic inclusion particles containing TiN in this steel was concluded as described below. During the deoxidization occurred by addition of Al, the phase consisted of Al_2O_3 and AlN was separated from the melting steel. After that, during the denitrified by addition of Ti, the TiN phase was deposited on the inclusion consisted of Al_2O_3 and AlN.

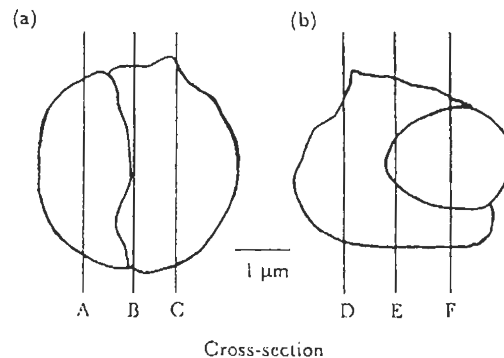

Fig. 5 Sketches of the analyzed inclusion particle in cluster 2.

Table Composition in the cross-section area in Fig. 5, (a) particle A, (b) particle B.

Particle	Cross-section	Al_2O_3	AlN	$Na_2O{\cdot}2SiO_2$	TiN
A	Section A	85.3	10.2	1.3	3.2
	Section B	83.7	11.5	1.0	3.8
	Section C	84.9	7.7	1.2	6.2
B	Section D	87.6	5.2	6.0	1.2
	Section E	86.1	2.4	7.4	4.1
	Section F	86.9	1.8	6.9	4.4

(mass%)

3.3 X-ray Photo- and Auger Electron Diffraction with High-angular-resolution

The Mg $KL_{2,3}L_{2,3}$ two-dimensional diffraction pattern observed for the clean MgO(001) surface is shown in Fig. 6. A great number of very fine features were clearly observed in the diffraction pattern. Many dark lines can be distinguished in the pattern which have not been clearly observed previously. The more intense dark lines were observed at the border of the bright region of bands. These features are similar to the Kikuchi bands observed in transmission electron diffraction, and reflection high-energy electron diffraction. Other less pronounced dark lines could also be observed.

In order to interpret the features of the observed pattern, we tried matching the dark lines with geometrically calculated lines. The dark lines were matched with the projected lines of a cone onto a spherical surface. The two-dimensional map is the projection of the Mg $KL_{2,3}L_{2,3}$ intensities on the spherical surface. A match between the dark lines and the projected lines was obtained by three-parameter (α, β, γ) fitting calculations.

In Fig. 7, solid lines show the result of matching the dark line-pairs at the border of the bright region of bands. The calculated first and second -order Bragg lines are shown as broken lines. Thus, dark lines pairs seem to be related to the Bragg diffraction associated with low index planes. Some dark lines associated with higher index, e.g. (240), Bragg diffraction are also distinguishable.

The cross-sectional feature of a band (from point P to point Q in Fig. 7) is shown in Fig. 8. In Fig. 8, the solid lines and the broken lines represent the position of the observed dark lines and the calculated first-order Bragg angles corresponding to the (220) planes, respectively. The variation of the intensity of photo- and Auger electron near the Bragg angle is very similar to that of Kikuchi bands

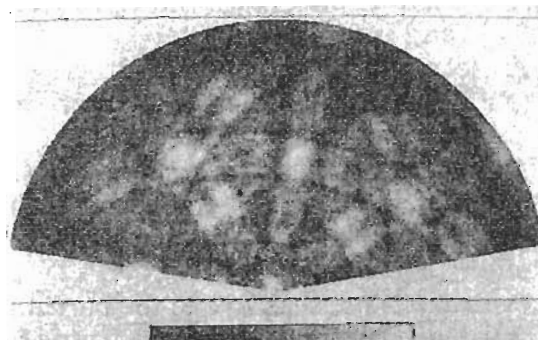

Fig. 6 Mg $KL_{2,3}L_{2,3}$ X-ray excited Auger electron (1182eV) diffraction pattern from a MgO(001) surface.

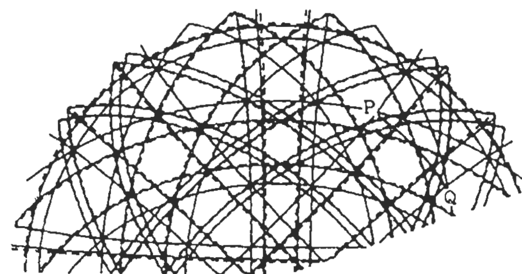

Fig. 7 Solid lines show the result of matching of the dark line pairs at the border of the bright region of bands. Broken lines show the projection of Bragg angle of the low index planes.

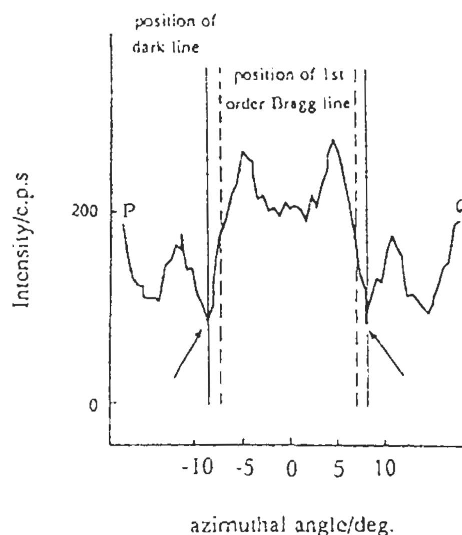

Fig. 8 Cross section of the band from point P to point Q in Fig. 7.

observed in electron diffraction experiments. These kinds of analysis of the fine structures of photo- and Auger electron diffraction not only reveal the essential character of this phenomenon but also promote the application of this to the structural analysis of the surface layer with high precision.

3.4 X-ray Photoelectron Diffraction Studies on Ultra Thin Epitaxial Films and Interfaces

A lot of X-ray photoelectron diffraction (XPED) measurements have been made for characterizing epitaxial structures. In such studies, strong forward scattering peaks along interatomic axes between photoelectron emitters and their neighboring atoms have been effectively used. However, XPED from an overlayer is not sensitive to the buried interface structure, because strong forward scattering inside the overlayer is dominant and backscattering from the underlying substrate is small. On the other hand, in a heteroepitaxial system including a buried interlayer with an element which is not found in both the overlayer and the substrate, the interface structure is characterized effectively with forward scattering peaks in angular distributions of photoelectrons emitted from the interlayer atoms.

As an example of this kind of analysis, our recent results for CaF_2 ultra thin films grown on the sulfur-passivated InP(100) are considered[9,10]. In Fig. 9(a), polar angle distributions along the [010] azimuth for three core levels, $In3d_{5/2}$, Ca2p and S2p from the substrate, the overlayer and the interlayer, respectively are presented. All data are compared with multiple scattering cluster calculations with spherical wave scattering (MSC-SW). First, the polar scan of $In3d_{5/2}$ was calculated for the bulk structure of InP(100) and compared with the experimental scan obtained before CaF_2 deposition. As shown in Fig. 9(a), the agreement between experiment and theory is very good. Next, for the structure of the CaF_2 overlayer, since the prominent forward scattering peaks in the polar scan of Ca2p can be correlated to the crystal axes of the CaF_2(100) crystal as shown in Figs. 9(a) and 9(b), it is easy to see that CaF_2(100) can grow epitaxially on S/InP(100). In addition, one observes the peaks near q=0°, 45° and 70° even at a coverage of 1.0 DL-EQ(double-layers equivalent). As shown in Fig. 9(b), the peak at θ = 0° is due to forward scattering of electrons generated in the first Ca layer by atoms in the third Ca layer. Therefore, it is obvious that CaF_2 grows in the island mode and that at least a local third double-layer of CaF_2 is grown even

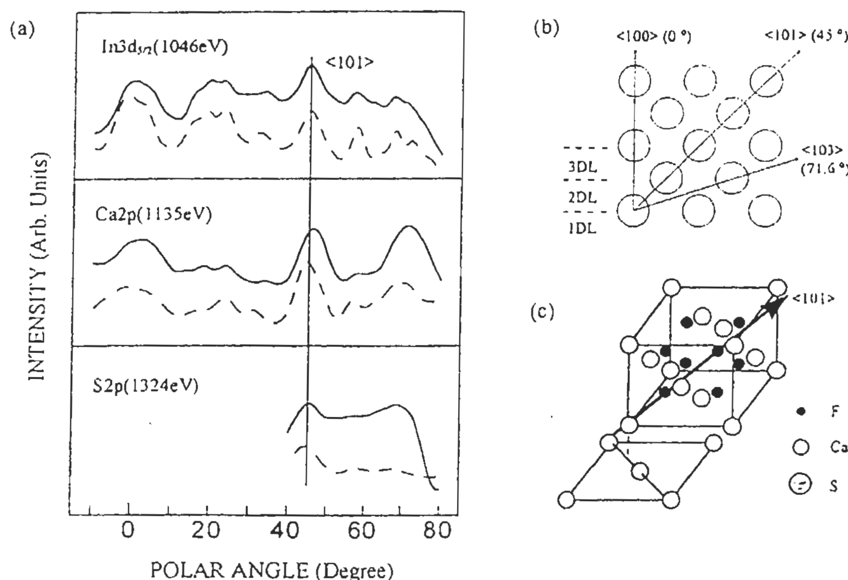

Fig. 9 (a) Experimental (solid curves) and theoretical (dotted curves) polar scans of $In3d_{5/2}$, Ca2p and S2p intensities for the CaF_2 thin film at 1.0 DL-EQ grown on the S-passivated InP(100) substrate. (b) Structural models of the CaF_2 overlayer and the interface deduced from the XPED data. (c) Stacking models of CaF_2 overlayer on the S layer in S-passivated InP(100) substrate

at 1.0 DL-EQ. MSC calculation for the island cluster with the thickness of 3 DL reproduces the experimental curve quite well. Finally, the peak along <101> is observed in the polar scan of S2p, which indicates the direction of the interatomic axis between S atoms and their neighboring atoms at the interface. From this fact and MSC calculation, the possible stacking of the overlayer on the S layer is determined, as shown in Fig. 9(c). Since the agreement between experiment and theory is very good for all three XPED curves, our calculation method is reliable and can be used for characterizing other unknown structures.

4. Summary

A method for three-dimensional simulation of erosion of a solid by FIB bombardment was established. By this simulation, the property of the crosssectioning of a particle with shave-off scan was discussed. The result showed that there was little topographic effect in the shave-off scan, and this crosssectioning procedure is the most suitable for microparticle analysis.
Shave-off analysis was applied to nonmetallic inclusion particles in Al-deoxidized and Ti-denitrified low carbon steel. The inclusion particles were classified into 3 by EPMA and cluster analysis. It was verified that the $Na2O.2SiO_2$ phase existed in the particle. By the shave-off analysis, the average composition of any cross-sectional area in a particle was obtained quantitatively. We conclude that Ga-FIB SIMS is a very powerful tool for quantitative analysis of micro particles like a nonmetallic inclusion particle.
Many features originating from Bragg reflections by atomic planes have been clearly observed in the Auger electron diffraction pattern from the MgO(001) surface with high angular resolution of ±0.6° Geometric consideration of the directions of diffracted beams in the crystal was used to assign all features to specific low-index crystal planes. This kind of measurement is very important to clarify the basic scattering process in the surface.
Moreover, as an example of the application of XPED, the structural analysis of CaF_2 eptaxial layer grown on S-passivated InP(100) was introduced. In addition to the determination of the crystal structure and growth mode of the thin film, the XPED patterns from the interface layer of sulfur was effectively used to determine the stacking of the overlayer on the substrate. Thus, X-ray photoelectron diffraction is proved to be very useful for the structural analysis not only on the epitaxial overlayer, but also on the buried interface.

References

1. *Secondary Ion Mass Spectrometry SIMS IX*, eds. A. Benninghoven, Y. Nihei, R. Shimizu and H. W. Werner, (John Wiley & Sons, Chichester, 1994).
2. *Secondary Ion Mass Spectrometry SIMS X*, eds. A. Benninghoven, and H. W. Werner, (John Wiley & Sons, Chichester, 1997).
3. J. Bennett and D. Simons: J. Vac. Sci. & Technol. **A9** (1991) 1379.
4. H. Satoh, M. Owari and Y. Nihei: Jpn. J. Appl. Phys. **32** (1993) 3616.
5. Y. Nihei, H. Satoh, S. Tatsuzawa, M. Owari, M. Ataka, R. Aihara, K. Azuma and Y. Kammei: J. Vac. Sci. & Technol. **A5** (1987) 1254.
6. Y. Ichinohe, H. Ishii, M. Owari and Y. Nihei : J. Vac. Sci. Technol. **A13** (1995) 1489.
7. H. Satoh, M. Owari and Y. Nihei: J. Vac. Sci. & Technol. **B6** (1988) 915.
8. J. P. Ducommun, M. Cantegrel and M. Moulin : J. Mater. Sci. **10** (1975) 52.
9. S. Omori, H. Ishii and Y. Nihei, Surf. Sci., in press.
10. S. Omori, H. Ishii and Y. Nihei, Appl. Surf. Sci., in press.